Experimental Validation of an Active Wideband SSR Damping Scheme for Series-Compensated Networks

Tibin Joseph, *Member, IEEE*, Carlos E. Ugalde-Loo, *Member, IEEE*, Senthooran Balasubramaniam, *Member, IEEE*, Jun Liang, *Senior Member, IEEE*, and Gen Li, *Member, IEEE*

Abstract—Transmission network reinforcements are being undertaken to meet renewable energy targets towards a low carbon transition. High-voltage direct-current (HVDC) links and series-compensated ac lines are frontrunners in these developments. Although series capacitor installations can lead to subsynchronous resonance (SSR), HVDC links based on voltage source converters (VSCs) can be used to effectively damp SSR upon occurrence. An active damping technique to mitigate torsional interactions (TIs), a form of SSR, is presented. The damping scheme considers an active wideband filter to ensure positive damping in a wide range of subsynchronous frequencies. A state-space representation of the system has been formulated and eigenanalyses have been performed to assess the impact of the HVDC link on the TIs. A damping torque study for SSR screening is carried out, with results complemented with time-domain simulations to assess the accuracy of the small-signal models. The test system is implemented in a real-time digital simulator and connected to a VSC-HVDC scaled-down test-rig to validate the damping scheme through hardware-in-the-loop experiments. The presented damping method exhibits a satisfactory performance, with time-domain simulations and laboratory experiments showing a good correlation.

Keywords—*subsynchronous resonance, HVDC, eigenanalysis, damping torque, series compensation, active filter, VSC.*

I. INTRODUCTION

HIGH-voltage direct-current (HVDC) links and series compensation have been adopted as transmission network reinforcements to meet an increased electricity demand and renewable energy targets. However, these upgrades bring operability challenges to grid operators [1], [2]. Particularly, series compensation may produce an instability phenomenon termed subsynchronous resonance (SSR) [2]–[4].

SSR is an electric power system condition where the electric network exchanges energy with a turbine-generator at one or more of the natural frequencies of the combined system below the synchronous frequency [3]. Although SSR is a topic that has been studied for several years, it has lately attracted significant industrial attention. For instance, the threat of SSR in the Great Britain (GB) transmission system is considerable given the recent installation of series compensation near the Anglo-Scottish inter-tie (the so-called B6 boundary) in the quest to maximize bulk power transmission [2], [5].

T. Joseph, C. E. Ugalde-Loo, J. Liang, and G. Li are with the School of Engineering, Cardiff University, Cardiff, CF24 3AA, Wales, U.K. (e-mail: JosephT; Ugalde-LooC; LiangJ1; LiG9{@cardiff.ac.uk}).

S. Balasubramaniam is with Swansea University, Swansea, SA1 8EN, Wales, U.K. (email: s.balasubramaniam@swansea.ac.uk).

Network upgrades using HVDC links are an alternative to series compensation as they offer good reliability and controllability while providing additional services to network operators [1]. For example, in addition to fixed series capacitor banks and thyristor-controlled series compensators (TCSCs) being installed alongside, the 400 kV transmission network in the B6 boundary of the GB system has been reinforced with a submarine HVDC link at the West coast. An additional HVDC link is currently under construction at the East coast [2], [5]. However, a careful SSR assessment of new HVDC installations nearby series-compensated lines should be performed given that interactions between HVDC links and turbine-generators have been reported [6]–[8].

Traditional SSR mitigation schemes use filters placed either at the generator terminals or integrated with network components. Commonly employed generator-side mitigation measures include: passive filters tuned at specific subsynchronous frequencies (SSFs) [2], and supplementary excitation damping control (SEDC), where SSR damping is achieved by modulating the excitation voltage of the generator [9]. Recent notable examples include the use of 11 kV variable frequency drives enabled with a subsynchronous damping controller (SSDC) [10], and SEDC and torsional stress relay installed at the generator terminals for multi-modal SSR problems [11]. However, the aforementioned schemes are likely expensive as they are connected in series with the generator and, thus, should be rated to carry the full generator current [2].

The use of SSR damping measures at a transmission level is also common. Solutions include the use of blocking filters installed with series capacitors and tuned to counter resonant conditions [2]. Other schemes consider active filter based-SSDCs embedded in power converters of HVDC stations and flexible ac transmission systems (FACTS) devices [6], [12]–[18]. The addition of supplementary damping capabilities to an existing asset provides the most cost-effective solution for subsynchronous oscillation mitigation compared to other schemes [2], [6], [13]—arguably, the use of a power converter exclusively for damping purposes represents an asset under-utilization. However, most of the proposed controllers are designed for specific operating points and, thus, are sensitive to the system configuration and loading conditions. Although schemes for the real-time estimation and on-line monitoring of SSF components may relieve the aforementioned issues [18], [19], they could be computationally intensive. For instance, even when [20] represents a good attempt to experimentally damp SSR, the practical contribution of the work is limited as the time to detect SSR and the precision of frequency estimation depend on the signal processing method used for the analysis of the input signal.

Active damping provided by power converters connected at

the generator side has been also explored. For instance, a voltage source converter (VSC) topology for damping services and reactive power modulation of VSCs to damp subsynchronous oscillations have been reported [21], [22]. In these schemes, the generator (or turbine) speed is used as an input signal to the SSDC, communication links are required to transfer such signal to the physical location of the SSDC, and active filters are required for SSR damping. However, communication failure or delays may affect the reliability of the scheme, which is undesirable due to the instability risks posed by SSR. Therefore, the use of local signals is preferred for damping when the compensating device providing the service is located physically far from the generator [6], [10].

In general, most damping schemes reported in the literature employ active filters tuned for specific torsional modes (TMs). However, different TMs may be excited depending on the series compensation level—limiting the adaptability of the schemes [19]. Additionally, active filter-based solutions may introduce undesired negative damping at sideband frequencies [16]. Taking into account the previous considerations, a wideband filter based damper (WBD) which can damp multiple TM frequencies is developed in this work. The paper builds on the efforts in [16] by assessing the performance of WBD-embedded HVDC links and their capability to concurrently provide power transfer and auxiliary SSR damping functionalities within their existing capacity. The proposed damper can be used regardless of system configuration and series compensation level. Eigenvalue and damping torque analysis are used to identify instability regions and to assess the effectiveness of the WBD-based SSDC. The damping performance upon small and large disturbances is verified through time-domain simulations. To assess and to validate its real-time operation, the SSDC is implemented in an experimental test-rig and hardware-in-the-loop (HiL) experiments are performed.

It should be emphasized that the scope of this work is on torsional interactions (TIs)—a type of SSR that may cause stress, fatigue, and ultimately failure and damage to the shafts [2], [4]. At least initially, TI is a small disturbance condition where a sustained torque oscillation arises due to the interplay between the electrical modes of series-compensated lines with the mechanical modes of nearby thermal generation plants. The reader is referred to [3], [4] for further information on other types of SSR. In addition to SSR phenomena, other type of subsynchronous interactions exist, such as the subsynchronous torsional interactions (SSTIs). As opposed to TIs, SSTIs do not involve series compensation. Instead, they arise from the incorporation of power converters into a power system and their interaction with turbine-generator shafts [5]. SSTI may result in shaft oscillations—although at a smaller scale than when TI occurs. Given that the focus of this paper is on series-compensated systems, the study of SSTIs is not considered.

II. System Configuration under Study

A. Reduced Great Britain Transmission Network

The three-machine model of the GB transmission system is used. The system is divided into three generation areas: Southern Scotland (SS), Northern Scotland (NS), and England and Wales (E&W), with ratings shown in Fig. 1. Although it is arguably a simplified version of the GB system, it has
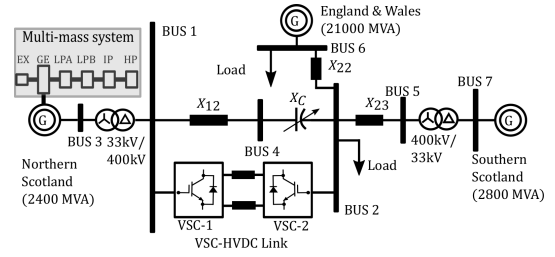

Fig. 1. Three-machine GB system model with reinforcements.

been previously employed for SSR studies [13], [20], [24], [25]. Despite its simplicity, it provides sufficient information to study and understand the SSR phenomena and to elucidate key concepts by reducing system complexity while keeping an appropriate weighting of the size of generation.

The model was originally designed in consultation with National Grid, the GB transmission system owner and operator, to resemble the operating conditions of mainland GB [13], [26]. It has been upgraded to consider onshore and offshore infrastructure reinforcements to facilitate the transmission of additional wind power from Scotland to major load centers in the South without the construction of new overhead lines. Network upgrades are included as follows: the transmission line connecting the NS generator features series compensation and a VSC-HVDC link is connected between Buses 1 and 2. The NS generator considers a multi-mass shaft representation with six turbine masses. The SSR threat faced by the practical GB system is thus encapsulated in the model—emulating thermal generation plant in the proximities of the series compensation installations. The other machines were modeled as generators with a single mass shaft representation [27].

Although shaft dynamics are key for TI analysis, it should be emphasized that there is a lack of availability of shaft data for the GB power system [5], [28]. Despite this shortcoming, the shaft representation adopted in this work considers a realistic range of TM frequencies [29]. In addition, levels up to 35% of series compensation have been deemed as safe from SSR—in line with frequency scanning studies conducted by National Grid and Scottish Power Energy Networks [30]. Even when aggregated generator models have been adopted, a quick characterization of the SSR phenomenon can be performed, damping schemes tested, and the lessons learned can be readily be transferred to the practical power system itself—in the same manner as it has been conventionally done through the use of classical IEEE benchmark models for SSR studies [31], [32].

B. VSC-HVDC Link Modeling

The HVDC link is operated primarily to transmit active power and to provide reactive power support at the point of common coupling. Fig. 2 illustrates the control strategy. The variables to be controlled are active and reactive power for the
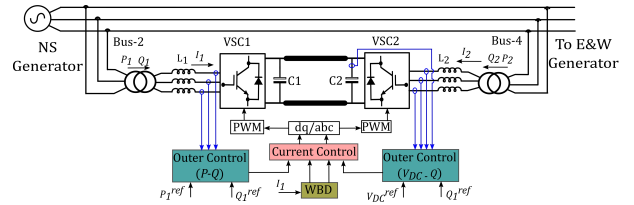

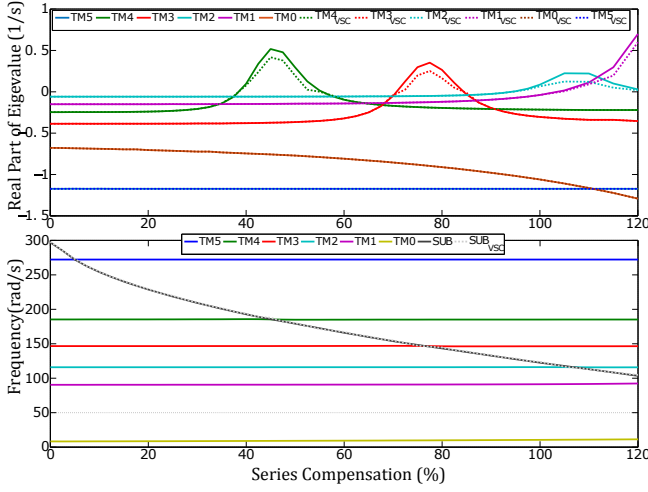Fig. 2. VSC-HVDC link with control loops.

Fig. 3. TM stability range in terms of series compensation percentage.

TABLE I. RELEVANT EIGENVALUES

TM Modes	30% Compensation $\sigma \pm j\omega$	40% Compensation $\sigma \pm j\omega$	75% Compensation $\sigma \pm j\omega$
TM5	$-1.173 \pm j272.193$	$-1.173 \pm j272.183$	$-1.173 \pm j272.193$
TM4	$-0.207 \pm j185.488$	$+0.097 \pm j187.925$	$-0.185 \pm j185.099$
TM3	$-0.383 \pm j146.666$	$-0.379 \pm j146.56$	$+0.297 \pm j146.825$
TM2	$-0.058 \pm j115.970$	$-0.058 \pm j114.75$	$-0.051 \pm j116.012$
TM1	$-0.149 \pm j90.574$	$-0.147 \pm j91.123$	$-0.128 \pm j90.868$
SUB	$-7.443 \pm j209.289$	$-7.674 \pm j191.574$	$-7.735 \pm j148.310$
SUPER	$-8.518 \pm j418.520$	$-8.665 \pm j432.55$	$-9.110 \pm j479.435$

rectifier terminal (VSC1) and dc voltage and reactive power for the inverter terminal (VSC2). For the detailed modeling of the HVDC link with associated controllers, the reader is referred to [25], [33]. The control parameters are included in the Appendix for completeness.

III. SSR ANALYSIS

A. Eigenvalue Analysis

A state-space model of the system shown in Fig. 1 has been developed. It considers the dynamic equations of the synchronous machines, transmission lines, and HVDC link. This is a system of 77 differential equations linearized around an operating point (not included due to space limitations). The results shown in this section were presented in [20]; however, they are reproduced here for completeness of the SSR analysis.

The state equation and state vector are given by

$$\Delta \dot{X}_{sys} = A_{sys} \Delta X_{sys}, \qquad (1)$$

$$\Delta X_{sys} = [X_{NG}, X_{N\omega}, X_{N\theta}, X_{SG}, X_{EWG}, X_T, X_{VSC}]^T, \quad (2)$$

where X_{NG}, $X_{N\omega}$, and $X_{N\theta}$ constitute the states associated with the NS generator; X_T the series-compensated transmission line; X_{SG}, X_{EWG} the SS and E&W generators; and X_{VSC} the VSC-HVDC link.

To perform eigenanalysis, system (1) has been constructed in MATLAB. The unstable TMs (TM1-TM4) related to the shaft of the NS generator may be excited at different levels of series compensation. The ranges for which torsional instability arises are shown in Fig. 3. System stability is directly related to the subsynchronous mode of the series-compensated transmission line linked to the NS generator (termed SUB). Instability occurs whenever SUB is in the vicinity of the frequencies of TM1-TM4—evidenced by the real part of the eigenvalues.

Relevant eigenvalues for 30, 40 and 75% series compensation of the transmission line connecting Buses 1 and 2 are summarized in Table 1. The system is stable for 30% of compensation—in line with [30]. However, for 40%, SUB ($\simeq 30.7$ Hz) interacts with TM4 of the shaft ($\simeq 29.6$ Hz). As a consequence, SSR arises and TM4 becomes unstable, evidenced by the positive real part of the eigenvalue. Similarly, for 75%, SUB ($\simeq 23.61$ Hz) interacts with TM3 ($\simeq 23.37$ Hz), as shown by the corresponding eigenvalue. Upon such conditions, faults and scheduled / unexpected switching actions may result in oscillations, rendering the system unstable.

The rationale for selecting the arguably high compensation level of 75% is to analyze the WBD performance under an extreme operating condition. Such a level of series compensation is not unrealistic as it has been implemented in practical installations—as reported in [17], [34]–[36].

B. Damping Torque Analysis

To verify the eigenanalysis, an EMT-based electrical damping analysis is performed. A distinctive feature of this method over eigenanalysis is that the VSCs are modeled in detail with all their components—including switches and delays associated with the valves [6], [37]. In addition, the contribution made by the VSC-HVDC link towards the electrical damping of the nearby generator unit can be assessed.

In general, the electromagnetic torque of the generator is:

$$T_e = P_e/\omega_r = T_{e0} + \Delta T_e, \qquad (3)$$

where P_e is the electrical power, T_{e0} is a constant torque depicting the generator output power at the fundamental frequency, and ΔT_e is the perturbed electromagnetic torque from torsional oscillations. ΔT_e is divided in two components:

$$\Delta T_e = T_s \Delta \theta + T_d \Delta \omega. \qquad (4)$$

The synchronizing torque component $T_s \Delta \theta$ acts as an auxiliary spring on the rotor and is in phase with the angular displacement. The damping torque component $T_d \Delta \omega$ acts as a damping element and is in phase with the angular velocity. Substituting $\Delta \theta = \Delta \omega / j\omega$ yields

$$\Delta T_e = \left(\frac{T_s}{j\omega} + T_d \right) \Delta \omega. \qquad (5)$$

The electrical damping factor can be obtained with (5) using the electrical torque and machine speed. To this end, a perturbation signal is injected to produce a small fluctuation in the turbine speed $\Delta \omega$. Electrical damping can be assessed by quantifying the resulting perturbation in electrical torque ΔT_e. Consider a perturbation signal modulated at frequency f_{mf}:

$$\omega(f_{mf}) = A_1 \sin(2\pi f_{mf} + \phi_1), \qquad (6)$$

where A_1 is the magnitude and ϕ_1 the phase angle of the injected perturbation signal. The corresponding electrical torque component $T_e(f_{mf})$ is given as

$$-T_e(f_{mf}) = B_1 \sin(2\pi f_{mf} + \phi_2), \qquad (7)$$

where B_2 and ϕ_2 are the magnitude and phase angle of $T_e(f_{mf})$. The damping factor D_e (or T_d) is computed as

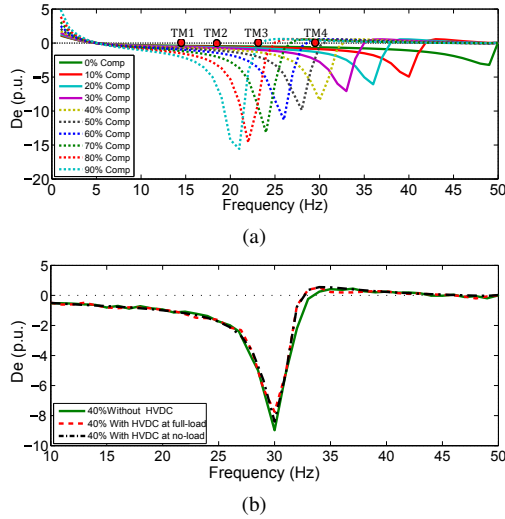$$D_e = \frac{B_1 \cos(\phi_2 - \phi_1)}{A_1}. \qquad (8)$$

Fig. 4. Electrical damping profile of the GB system: (a) for different series compensation levels; (b) to assess the impact of the VSC-HVDC link.

If D_e in (8) is positive for the entire subsynchronous range, there is low-risk of SSR. Conversely, negative values of D_e indicate the possibility of SSR occurrence [6], [37].

An SSR screening for the system in Fig. 1 was done, with results shown in Fig. 4(a). A perturbation was applied for the whole subsynchronous range (0 to 50 Hz) using (6). The selection of A_1 was made carefully to avoid affecting the system's steady-state operation, with $A_1 = 0.001$ p.u. The disturbance was applied with the system in steady-state and the damping factor recorded after a few cycles. The compensation level was varied from 0 to 90%. The TMs of the NS generator as identified from the eigenanalysis are shown with red circles. The damping torque traces reveal the levels of compensation at which the maximum interaction takes place. This occurs for frequencies in the TMs' vicinity—for compensation levels of 40, 75, and $> 90\%$. Moreover, it is clearly seen that a greater risk of SSR is associated with high compensation levels.

To further evaluate the impact that the HVDC link has on SSR, the damping profile of the GB network at 40% of series compensation is evaluated for three different conditions. The cases correspond to the test system without an HVDC link, with an HVDC link connected and operated at no-load, and with an HVDC link connected at full-load. Results are shown in Fig. 4(b). It can be seen that the negative peak slightly diminishes when the HVDC link is in service—irrespective of the loading condition. However, the HVDC link cannot sufficiently increase the network damping by itself under maximum TIs—such as the one occurring at 40% of series compensation. Although the damping torque increases with an increase in the loading condition, this effect can be considered as negligible when it comes to its contribution to SSR damping.

IV. WIDEBAND DAMPING APPROACH

As shown in Section III, a VSC-HVDC link by itself neither affects system stability nor substantially contributes to system damping. However, its control flexibility may be exploited to provide ancillary services. Following this line, a WBD embedded in a VSC station of the HVDC is presented as an auxiliary controller to damp SSR upon occurrence.
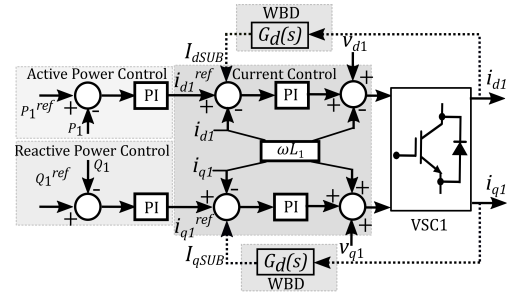

Fig. 5. VSC control structure upgraded with a WBD (rectifier terminal).

The WBD scheme presented in this section provides positive damping in a wide range of frequencies within the subsynchronous region (15-30 Hz), which coincides where the TMs of turbine-generators within the GB system lie [29]. Since these modes of oscillation are fixed as long as the generator rotor or turbine blades are not replaced [38], a properly designed WBD may achieve sufficient damping for the entire frequency range of interest irrespective of changes in the configuration of the transmission network—with minimal impact on the operation of the HVDC system. Damping is deemed sufficient if the magnitude of speed oscillations or rotor angle drops to less than 15% of the peak deviation in the following 20 s of a disturbance, as established by National Grid [2].

Fig. 5 shows the control structure of a WBD-upgraded VSC. The injection point for the damping signal has been selected to provide a faster action on the negative damping associated with the SSF components of interest upon an SSR event. This is achieved by processing the line current (in a dq frame) through a compensator $G_d(s)$ to generate current components I_{dSUB} and I_{qSUB}. These are used, in turn, to modulate the active and reactive current references of VSC1 (i_{d1}^{ref}, i_{q1}^{ref}).

The WBD adopted in this paper has the form

$$G_d(s) = k_{WBD} \cdot \frac{s\left(\dfrac{\omega_c}{Q}\right)}{s^2 + \left(\dfrac{\omega_c}{Q}\right)s + \omega_c^2} \qquad (9)$$

which is a second order bandpass filter, where ω_c is the center frequency, Q the quality factor, and k_{WBD} the filter gain. The WBD should follow relevant TMs and allow for a zero phase shift around ω_c.

The WBD in (9) is embedded in the VSC control system (see Fig. 5). The value of ω_c is selected first based on the locations of the TMs of the turbine-generator—which are constant and typically in the range of 15 to 30 Hz (94 to 188 rad/s). The damper design is easy if the TMs to be damped are known beforehand. However, if prior knowledge of their exact location is not available, it is recommended to select ω_c as the middle value in the aforementioned frequency range [16].

For the test system adopted in this paper, the selection of ω_c has been made under the assumption that the TMs are known. As concluded through eigenanalysis (see Section III-A), TM3 (26 Hz) and TM4 (20 Hz) correspond to 75 and 40% of series compensation and, thus, the center frequency is selected as $\omega_c = 150.72$ rad/s ($2\pi \times 24$ Hz).

Once ω_c is determined, care should be exercised when selecting Q and k_{WBD}. To ensure an adequate damping
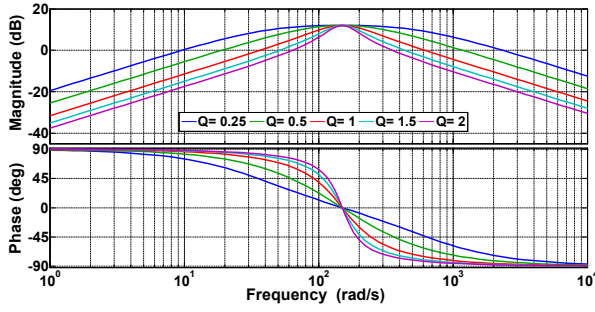
Fig. 6. Frequency response of $G_d(s)$ for different values of Q ($\omega_c = 150.72$ rad/s, $k_{WBD} = 4$).
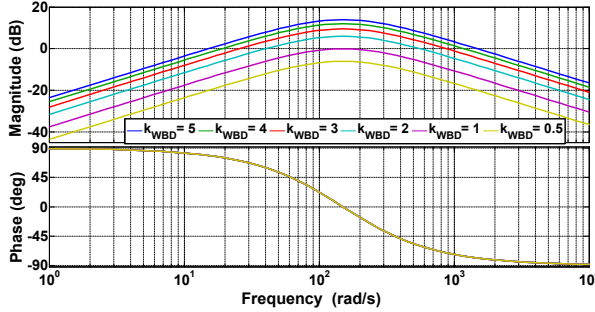

Fig. 7. Frequency response of $G_d(s)$ for different values of k_{WBD} ($\omega_c = 150.72$ rad/s, $Q = 0.5$).

performance over the SSF range of interest and to minimize the impact on the normal operation of the HVDC system, a magnitude of $|G_d(s)| > 10$ dB at ω_c is recommended—which can be achieved through the suitable selection of k_{WBD} [16]. On the other hand, the passband range is determined by Q. A large value of Q would lead to a narrow band for frequencies to be damped and, conversely, a small value increases the width of the band. As a rule of thumb, large values of Q and k_{WBD} should be avoided as different TMs may be triggered.

A parametric study is carried out to select Q and k_{WBD}. Fig. 6 shows the frequency response of $G_d(s)$ for different values of Q, whereas Fig. 7 considers parametric variations in k_{WBD}. As it can be observed, the selection of Q and k_{WBD} has a significant impact on the frequency characteristics of the damper. Based on the frequency responses provided by Figs. 6 and 7, the remaining design parameters of (9) are chosen as $Q = 0.5$ and $k_{WBD} = 4$. The resulting WBD is given as

$$G_d(s) = \frac{1200s}{s^2 + 300s + 22500}, \qquad (10)$$

which has a magnitude over 10 dB at the center frequency and a frequency band wide enough to damp the TMs of interest. This filter structure is kept for both the simulation and experimental results presented in subsequent sections.

To gain further insight into the damping contribution afforded by the WBD-enabled VSC, the electric damping profiles for the system under study with 40 and 75% series compensation are shown in Fig. 8. As it can be observed, a negative electrical damping profile results when the WBD is not in operation, with large negative peaks centered at the location of TM3 and TM4. This is consistent with the eigenanalysis in Section III, as SSR is exhibited for such values of series compensation. However, when the WBD is in service
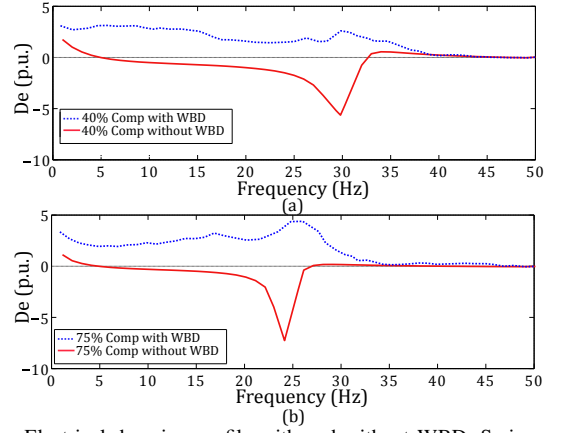

Fig. 8. Electrical damping profile with and without WBD. Series compensation of (a) 40%; (b) 75%.

TABLE II. RELEVANT EIGENVALUES OF THE SYSTEM WITH WBD

TM	40% Compensation	75% Compensation
TM5	$-1.173 \pm j272.183$	$-1.173 \pm j272.192$
TM4	$-0.738 \pm j185.613$	$-0.282 \pm j183.112$
TM3	$-0.379 \pm j144.561$	$-0.562 \pm j143.914$
TM2	$-0.066 \pm j117.89$	$-0.054 \pm j115.210$
TM1	$-0.139 \pm j90.521$	$-0.112 \pm j89.931$
SUB	$-2.631 \pm j229.930$	$-1.443 \pm j227.832$
SUPER	$-6.325 \pm j436.238$	$-7.012 \pm j480.198$

a positive damping is provided instead at frequencies around the TMs. This implies that the system is being compensated at critical frequencies and stability is preserved.

To support the previous analysis, the relevant eigenvalues of the WBD-upgraded system are summarized in Table II. As it can be observed, the frequency of SUB shifts away from that of TM3 and TM4 if the damper is in operation. As a result, the system is stable, with TM3 and TM4 now exhibiting a negative real part (see Table I for comparison with the system without WBD). These results verify that the proposed approach is able to stabilize multiple TMs of the GB system model.

Note: It should be highlighted that the adopted approach offers advantages over passive filter-based schemes. For instance, modal filter-based schemes require a precise knowledge of the shaft dynamics. Separation filters, associated phase shifters and compensation gains for each TM are also needed [16]. As a result, extensive studies are required to ensure the effectiveness of the scheme across a wide range of operating conditions [38]. If a single TM is targeted, the filter may need to be re-tuned following transmission network changes as other TMs may be excited. Adaptive schemes may relieve these issues, but they bring an economic burden to asset owners as each generator unit would require separate filter banks.

Instead of designing filters for each TM and by-passing other modes, the WBD does not require further re-tuning to act on multiple TMs since the design accounts for a wide frequency band of operation. Damping will be provided irrespective of the network configuration or operating condition since the TMs remain fixed. In addition, given the uncertainty around key shaft data in the GB system (e.g. inertia constants, torsional stiffnesses, damping coefficients), the WBD-based solution is of practical relevance. Although it may be interesting to compare the performance of a modal-based approach against the WBD scheme, this falls out of the scope of the paper.

V. TIME-DOMAIN RESULTS

To verify the damping torque analysis and WBD design, time-domain simulations of the system shown in Fig. 1 have been carried out in PSCAD/EMTDC for both small and large disturbances. Results have been obtained for a WBD-upgraded VSC and when the WBD is not in service.

A. Small Disturbance Analysis

A small disturbance is achieved by modifying the series compensation level (*i.e.* value of X_c). A level of 20% is initially selected to ensure that the system is stable and in steady-state—as suggested by Fig. 3. Simulations are performed for changes in compensation to 30, 40, and 75% at $t = 4$ s, with results shown in Fig. 9 when the WBD is not employed. As it can be observed, the system remains stable for 30% compensation, as expected. However, for changes to 40 and 75%, the system becomes unstable—evidenced by the growing oscillations in torque (Figs. 9(a)-(b)), dc power (Fig. 9(c)), and frequency (Fig. 9(d)). Such torque responses would eventually damage a generator shaft if corrective measures are not taken.

Changes in compensation level to 40 and 75% cause the current of the NS generator to deviate from its normal operating condition, as evidenced in Fig. 10(a)-(b). Fig. 10(c)-(d) show the fast Fourier transform (FFT) of the line current, where SSF components for 40% (at 20 Hz) and 75% (at 26 Hz) compensation are observed. These components are the complements, respectively, of the frequencies of TM4 ($\approx$30 Hz) for 40% and TM3 ($\approx$24 Hz) for 75%. These results are consistent with the information provided by Fig. 3 (summarized in Table I) and with the damping profile in Fig. 4, as for 40 and 75% compensation the real parts of TM4 and TM3 become positive, respectively—hence representing unstable conditions. Moreover, the results clearly show that the VSC on its own does not provide sufficient system damping following a change in compensation. Without proper countermeasures in place, system operation could be compromised due to SSR.

Simulations are repeated for a WBD-upgraded VSC. Its contribution to SSR damping is examined by changing the compensation level from 20 to 40% at $t = 4$ s and subsequently to 75% at $t = 18$ s. Selected torque responses are shown in Fig. 11(a)-(c), with the network frequency provided in Fig. 11(d). As it can be observed, the inclusion of the damping controller prevents SSR from developing. Fig. 12(a) shows the successful mitigation of SSF components in line currents, which is further corroborated by the FFT spectrum of the line current for 40 and 75%, as shown in Fig. 12(b)-(c).

Fig. 13 shows the HVDC link dynamics when the WBD is employed. As it can be observed, fluctuations in dc voltage (V_{dc}) are negligible upon changes in series compensation (see Fig. 13(a)). The active power (P_1) is modulated around 4% to achieve a satisfactory damping performance (see Fig. 13(b)). SSR damping is achieved with the injection of SSF dq current components of a similar magnitude (I_{dSUB} and I_{qSUB}), as shown in Fig. 13(c). It should be emphasized that the magnitude of the injected damping currents before the disturbances is zero; however, as the level of series compensation is changed this increases to 0.25 kA (0.12 p.u.), which is then brought back to zero by the WBD-enabled VSC. The additional transients due to the modulation in dc power and

voltage are within the converter capability and do not affect the normal operation of the HVDC link.
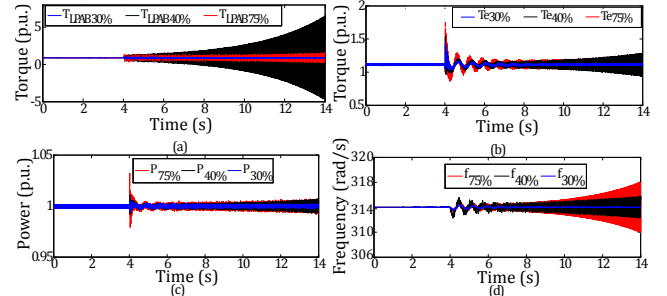

Fig. 9. Small disturbance simulation results without a WBD in service: (a) mechanical torque between low pressure turbines A and B (NS generator); (b) electromagnetic torque (NS generator); (c) output power of VSC1; (d) frequency.
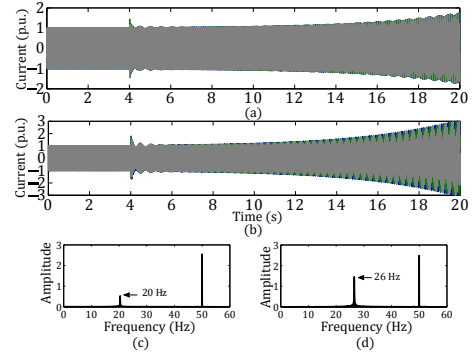

Fig. 10. Small disturbance simulation results without a WBD in service. Line current (phase a) for compensation level of: (a) 40%; (b) 75%. FFT spectrum of line current for compensation level of: (c) 40%; (d) 75%.

Fig. 11. Small disturbance simulation results with a WBD-enabled VSC in operation. Mechanical torque (NS generator) between: (a) high and intermediate pressure turbines; (b) low pressure turbines A and B; (c) electromagnetic torque (NS generator); (d) frequency.

Fig. 12. Small disturbance simulation results with a WBD-enabled VSC in operation. (a) Line current (phase a). FFT spectrum of line current for compensation level of: (b) 40%; (c) 75%.

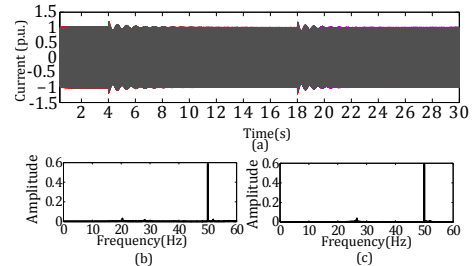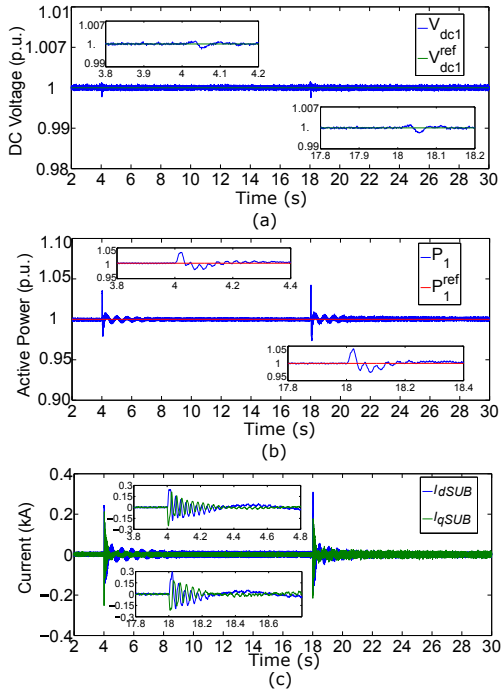Fig. 13. Small disturbance simulation results with a WBD-enabled VSC in operation. HVDC link dynamics: (a) DC link voltage; (b) output power at VSC1; (c) subsynchronous current dq components.

B. Large Disturbance Analysis

To assess system operation under a large disturbance, a three-phase-to-ground fault on the series-compensated line is simulated. The fault has a duration of 0.075 s and it occurs at $t = 4$ s into the simulation. A compensation level of 75% is considered. Results are shown in Fig. 14 both for a WBD-upgraded VSC and when the damper is not in operation. As it can be observed, system performance following fault clearance is compromised by SSR when the WBD is not active. However, an adequate system operation is exhibited when the WBD in VSC1 is enabled: mechanical torque oscillations decrease quickly (see Fig. 14(a)-(b)) and the dc link voltage and active power resume to the pre-fault condition (see Fig. 14(c)-(d)).

The results in this section confirm the capability of the WBD to damp SSR triggered by either small or large disturbances.

Note: The implementation of the WBD scheme presented in this paper focuses on TIs and other forms of SSR have not been considered. For instance, the induction generator effect (IGE) does not have a significant effect on TM stability [40], [41]. If IGE were to be analyzed, it could be approximately accounted for by inserting a negative resistance effect to subsynchronous currents in the transmission line. Existing literature has reported that in this case the network modes remain constant or fall within 15-30 Hz [42], which is incidentally the frequency range for which the WBD has been designed. Although it would be expected that the presented WBD scheme is capable of damping the oscillations induced by IGE, this falls out of the scope of this paper and requires further investigation.

VI. EXPERIMENTAL VALIDATION

To investigate the real-time operational characteristics of the WBD-based damping scheme, experimental tests are carried out on the multi-platform network shown in Fig. 15. These
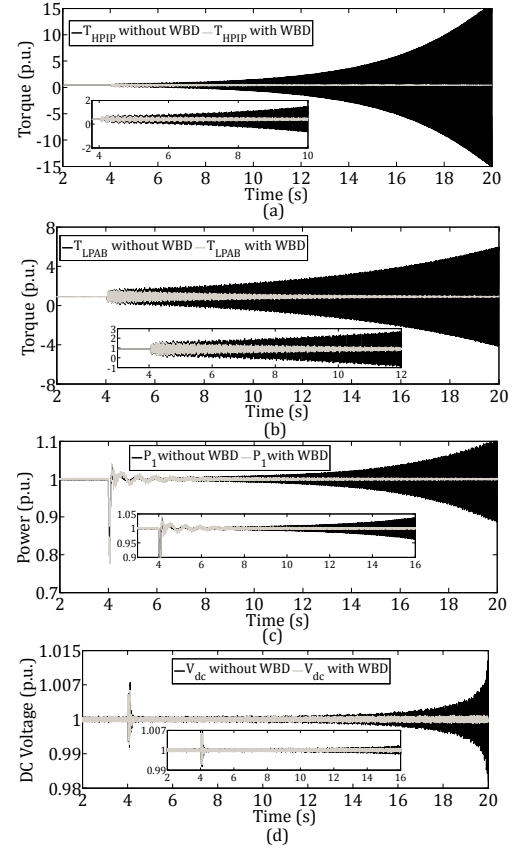

Fig. 14. Large disturbance simulation results with and without a WBD-enabled VSC in operation for 75% compensation. Mechanical torque (NS generator) between: (a) high and intermediate pressure turbines; (b) low pressure turbines A and B. (c) Output power at VSC1. (d) DC link voltage.

tests aim to assess the converter performance and its capability to achieve adequate SSR damping in the range of subsynchronous frequencies of interest.

A. Real-Time Hardware-in-the-Loop Configuration

Investigation of SSR and testing of damping schemes either in a practical power system or in a laboratory configuration is difficult and potentially dangerous [6], [39]. However, representative results can be achieved using an RT-HiL experimental platform. The platform adopted in this work consists of a real-time digital simulator (RTDS), a grid simulator (GS), and an HVDC test-rig. The connection of these components is depicted in Fig. 15(a). To perform the experiments, the three-machine GB system was modeled using the RSCAD software of the RTDS. This considers the turbine-generator models (including the multi-mass shaft representation for the NS generator), the transmission lines including series compensation, and loads, but does not include the VSC-HVDC link shown in Fig. 1. The HVDC is instead represented with the physical test-rig, which is built up using the VSC cabinets and dc network shown in Fig. 15(b). Both platforms are connected using the GS, which interfaces the analogue output (GTAO) cards of the RTDS firmware with the HVDC test-rig at suitable voltages.

The GS produces a three-phase mains supply voltage from the AO cards of the RTDS. This is achieved by using a four-quadrant amplifier rated at 2 kVA and 270 V (line-to-ground rms). To close the loop between the RTDS and the HVDC rig,

TABLE III.   RT-HiL PLATFORM: SPECIFICATIONS AND PARAMETERS

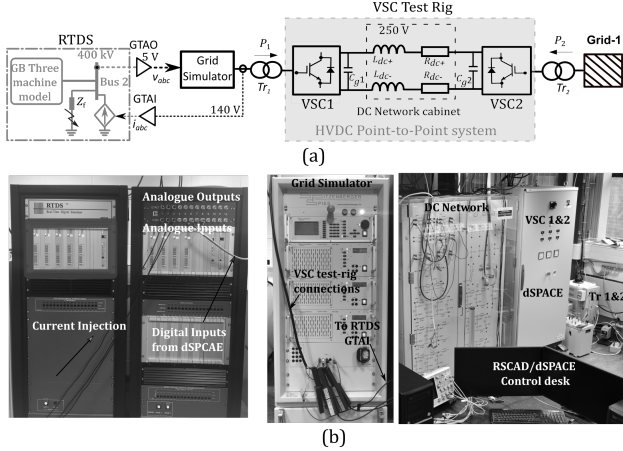| Devices	Specifications	Rating
Converters	Rated power	1 kW (1 p.u.)
	Rated ac voltage	140 V
	Rated dc voltage	250 V (1 p.u.)
	Topology	Two-level, symmetrical monopole
AC inductors	L_{g1}, L_{g2}	2.2 mH
DC lines	L_{dc}, R_{dc}	2.4 mH, 0.26 Ω
DC capacitors	C_{g1}, C_{g2}	1020 μF
Control system	dSPACE DS1005/ControlDesk 3.2 (Simulink interface)	
Real-time simulator	RTDS/RSCAD, Racks: 2. Cards: 2 GTWIF, 4 PB5 (2 GTDI, 2 GTDO, 2 GTAI, 2 GTAO, 2 GTNET)	

(a)

(b)

Fig. 15.   RT-HiL configuration: (a) Connection diagram; (b) physical set-up.

the three-phase line current is tapped and fed to the analogue input (GTAI) card of the RTDS.

The HVDC test-rig is formed by two VSCs, two transformers, and a dc network cabinet. The VSCs are operated at a rated power of 1 kW, 140 V ac and ±125 V dc. Through the GS, a conversion ratio of 400 kV / 140 V is achieved. A dSPACE platform is used to acquire data and monitor system states of the test-rig to control each VSC. The hardware set-up is shown in Fig. 15(b). Key parameters and specifications of the experimental platform are provided in Table III.

B. Experimental Results

The RT-HiL experiments were performed for a small disturbance. The experiment starts with the system operating in steady-state and 30% series compensation. The compensation level is increased to 40% at $t = 4$ s and subsequently to 75% at $t = 12$ s. Experimental results are shown in Fig. 16. As it can be observed, SSR is present if the WBD at VSC1 is not active (Fig. 16(a))—evidenced by the system frequency and selected torques between shaft sections. Conversely, SSR is effectively damped when the WBD is in operation irrespectively of the value of series compensation (Fig. 16(b)).

Fig. 17 shows the dc voltage and output power of VSC1 with and without the damping scheme in place. If no corrective measures are taken upon an SSR event, the magnitude of these variables would surpass the converter limits. Moreover, the system becomes unstable. Conversely, if the WBD is enabled, SSR is avoided. Notably, the damping service is provided without the need for overrating the converter—the dc voltage and power are within the converter capabilities. These results
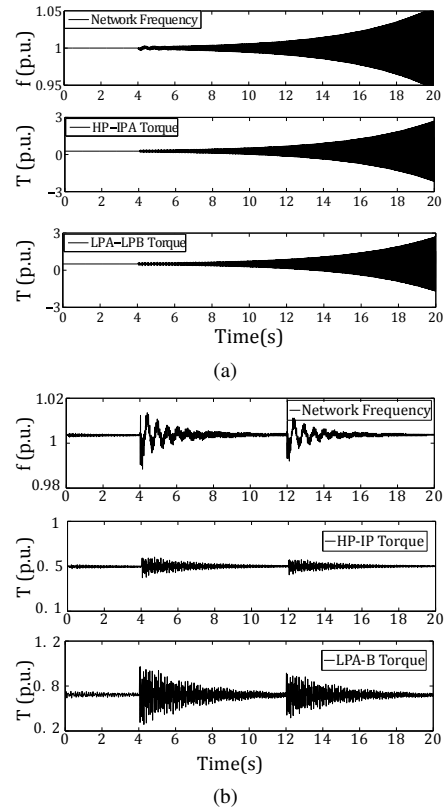

(a)

(b)

Fig. 16.   Experimental results (RTDS signals). Network frequency and mechanical torques (NS generator) between high and intermediate pressure and between low pressure turbines A and B: (a) without the damping scheme in place; (b) with the damping scheme activated.
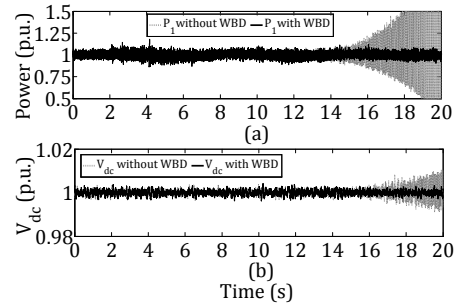

Fig. 17.   Experimental results (HVDC rig signals) with and without a WBD-enabled VSC in operation: (a) Output power at VSC1; (b) dc link voltage.

experimentally verify the analysis from Section III and validate the simulation results in Section V.

An additional experiment is carried out when the system is subjected to a large disturbance. To this end, a three-phase-to-ground fault is applied at the series-compensated line (*i.e.* modeled in the RTDS). A compensation level of 75% is considered. The fault is applied at $t = 4$ s for 75 ms on Bus 2 using a fault impedance Z_f (see Fig. 15(a)). Results are shown in Fig. 18. As it can be observed, the performance of the system after fault clearance is compromised due to SSR when the WBD is not in service—evidenced by the increasing oscillations in machine torques and dc link variables. However, the system successfully recovers when the WBD is in place.
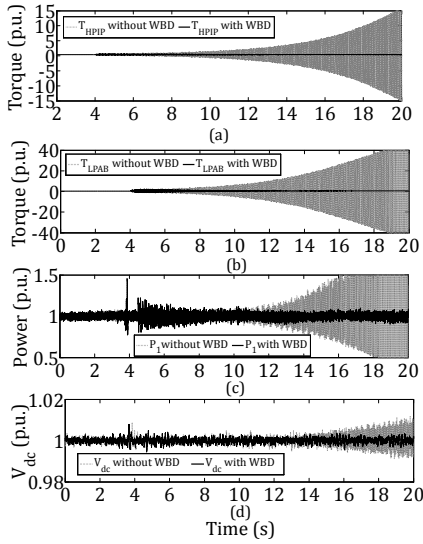
Fig. 18. Experimental results under a large disturbance. Mechanical torque (NS generator) between: (a) high and intermediate pressure turbines; (b) low pressure turbines A and B. (c) Output power at VSC1. (d) DC link voltage.
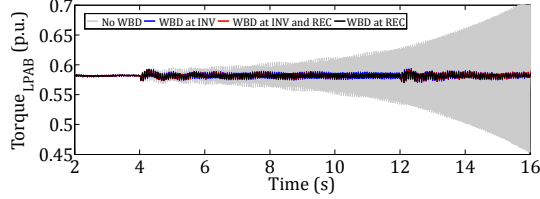

Fig. 19. Torque response of the E&W generator with and without WBD when a detailed shaft model is included.

VII. Damping Sensitivity and Limitations of the WBD-based Scheme

A. Impact of Generator Modeling and Damper Location

To further assess the performance of the WBD, a multi-mass shaft representation as in the NS generator has been included to the E&W generator (see Fig. 1). The WBD has been implemented in both converter stations of the HVDC link—in line with the approach being followed for the Western link [5]. Changes in series compensation take place from 20 to 40% at $t = 4$ s and then to 75% at 12 s into the simulation. The discussion is centered around the E&W generator.

Simulation results are shown in Fig. 19. As it can be observed in the torque response of the generator, the initial change in series compensation produces SSR if the WBD is not in service in either converter station. Conversely, damping is achieved when a WBD is active, irrespective of its location, or if the two WBDs are in service.

An additional simulation is carried out for the system in Fig. 1 (i.e. multi-mass shaft representation only in the NS generator), but the WBD is embedded into both terminals of the HVDC link. A change in compensation from 20 to 75% takes place at $t = 4$ s into the simulation (this would result in SSR for a system without the WBD being activated, as shown in Section V-A). Simulation results are given in Fig. 20.

Fig. 20(a) shows selected torque responses with the WBD in operation. As it can be observed, damping is preserved with the WBD installed only at the inverter terminal. However, the torque oscillations decay more slowly compared to when the
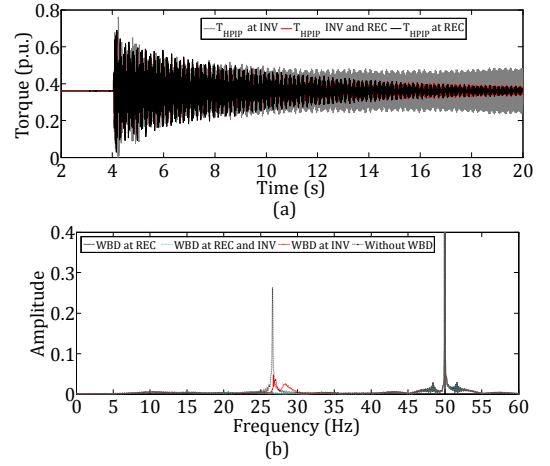

Fig. 20. Simulation results for 75% series-compensation with WBD at both converter terminals. (a) Mechanical torque (NS generator) between high and intermediate pressure turbines. (b) FFT spectrum of line current (phase a).
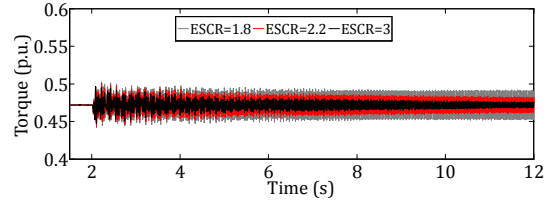

Fig. 21. Response for different ESCRs at 75% compensation with WBD.

WBD is active at the rectifier terminal only. Having the damper installed at both converters brings no substantial improvement, which is not unexpected due to the location of the multi-mass shaft. Fig. 20(b) shows the FFT spectrum of the line current of phase a, which supports the previous discussion.

It can be concluded from the results presented in this section that the location of the SSR damper should be chosen as close as possible from the vulnerable generators. If both terminals of an HVDC link are upgraded with the damping scheme, the VSC terminal closest to the affected generator should provide the damping services to achieve a better performance.

B. Impact of AC system Strength

The strength of the system is usually quantified with the effective short circuit ratio (ESCR), defined as [40], [43]

$$ESCR = \frac{S_{sc} - Q_{sc}}{P_{dc}}. \tag{11}$$

where S_{sc} is the short-circuit capability of the ac system, Q_{sc} is the total rated reactive power at the bus where an HVDC system is connected, and P_{dc} is the rated power of the HVDC system. If ESCR ≥ 2.5, a network is considered as strong.

It has been reported that network modes shift to higher frequencies if ESCR decreases [43]. Such a reduction is related to an increase in the transmission line reactance (X_l), which reduces the network's resonant frequency (ω_r) as $\frac{X_c}{X_l}$ decreases. This, in turn, has the effect of increasing the frequency of SUB as this is the complement of the resonant frequency (i.e. $\omega_0 - \omega_r$, where ω_0 is the fundamental frequency). However, SUB still lies within the range of the TMs.

A simulation is carried out to examine the impact of ESCR levels when the WBD is in service. The series compensation

level changes to 75% at $t = 2$ s into the simulation to produce SSR. As shown in Fig. 21, a low ESCR of 1.8 representing a weaker system does not have a severe impact on the damping performance compared to that of a stronger system with an ESCR of 3. In other words, the damping capability is still preserved for weak systems—at the expense of the affected generators exhibiting torque oscillations for a longer time.

C. Limitations of the WBD-based Scheme

Despite the advantages exhibited by the presented WBD-based scheme, care should be exercised prior to its adoption. For instance, the damping performance may be affected by the location of the HVDC converter terminal. Given that the scheme relies on the use of local measurements, damping will not be achieved quickly if the generator susceptible to SSR is far away. In this case, the growth of the torsional oscillations may not be reflected as quickly through remote voltage or current signals as it would through shaft speed measurements at the location of the affected generator. To relieve this shortcoming, the damping structure could be incorporated into any power electronics-based controller located in the vicinity of the generator—however, this requires further investigation that falls out of the scope of this paper.

On the other hand, the scheme may not be suitable to damp subsynchronous control interactions (SSCIs)—another form of subsynchronous oscillations arising when the modes of series-compensated transmission lines interact with control systems of power converters from FACTS devices or wind turbines [5], [44]. SSCI is a purely electrical phenomenon where the resonant frequency is not fixed and may fall outside of the frequency band considered by the WBD. Further work is required to suitably address SSCIs.

VIII. CONCLUSION

This paper has assessed the use of an SSR damping scheme based on an active wideband filter embedded in an HVDC link. Besides conducting a software-based verification of the scheme, this has also been experimentally validated, in real-time, using an HiL platform. Results show that the system operation under SSR events is not compromised and that damping can be contributed using the existing capacity of the converters in addition to the provision of bulk power transfer. The results obtained from simulation and experimental platforms exhibit a good correlation.

The damping scheme is applicable to any power system configuration. Despite its simplicity, it offers an effective performance without relying on communications or complex signal processing techniques. A significant advantage over other damping methods is its capability to damp multiple TMs within the SSF range—therefore mitigating the risks arising from uncertainty in the mechanical parameters of turbine-generators. In addition, the damper structure may be easily transferred to any other power converter-based equipment. This may be useful if an HVDC converter terminal is not located nearby a turbine-generator exposed to SSR. These characteristics make of the presented scheme an attractive solution towards practical deployment.

Besides experimentally demonstrating the suitability of the WBD-based scheme, possible design errors, interaction be-tween hardware components and fault diagnostics were assessed in a multi-platform experimental test-bed. Due to the system instability associated to SSR and the real-time nature of the experiments, there was always the latent risk of permanently damaging equipment. It is difficult and potentially dangerous to emulate unstable operating conditions such as SSR in practical power systems. The real-time configuration presented in this paper serves this purpose and, arguably, contributes to reducing operational risks by facilitating a controlled and safe environment for testing potentially catastrophic conditions.

IX. APPENDIX

A. VSC-HVDC Control System Parameters

The PI controllers are represented in the form: $K(s) = K_p + K_i/s$. Two-level VSCs: Current: $K_p = 50$, $K_i = 15000$. DC voltage: $K_p = 0.2$, $K_i = 200$. Active power: $K_p = 0.2$, $K_i = 200$. Reactive power: $K_p = 0.2$, $K_i = 200$.

B. Turbo-generator Parameters

Machine rating: England and Wales: 21000 MVA, 400 kV. Southern Scotland: 2800 MVA, 33 kV. Northern Scotland: 2400 MVA, 33 kV. Base frequency: $f_b = 50$ Hz, $\omega_b = 2\pi f_b$.
Synchronous generators (on base of machine rating): $R_a = 0.002$, $X_d = 0.17$, $X_q = 2.07$, $X_q' = 0.906$, $X_q'' = 0.234$, $X_d' = 0.308$, $X_d'' = 0.234$, $X_{mq} = 1.9$, $X_{md} = 1.96$, $\tau_{do}' = 6.08s$, $\tau_{do}'' = 0.0526s$, $\tau_{qo}'' = 0.0.353s$.
Multi-mass shaft (Northern Scotland generator): Inertias (in MWs/MVA): $H_{HP} = 0.0928$, $H_{IPA} = 0.1555$, $H_{LA} = 0.8586$, $H_{LB} = 0.8842$, $H_G = 0.8684$, $H_{EX} = 0.0342$
Self and mutual damping coefficients (in p.u. T/p.u. speed dev.): $D_H = D_I = D_{LA} = D_{LB} = 0.1$, $D_G = D_X = 0$, $D_{HI} = D_{IA} = D_{AB} = D_{BG} = 0.2$, $D_{GX} = 0.005$
Torsional stiffness (in p.u. T/rad): $K_{HI} = 19.303$, $K_{IA} = 34.929$, $K_{AB} = 52.038$, $K_{BG} = 70.852$, $K_{GX} = 2.822$
Single mass shaft (Southern Scotland and England/Wales generators): Inertias (MWs/MVA): $H_{SS} = 3.84$, $H_{EW} = 5.$; Damping coefficients (p.u. T/p.u. speed dev.): $D_{SS} = D_{EW} = 0.1$.

REFERENCES

[1] National Grid, Network Options Assessment Report 2017-18, U.K., Jan. 2018.

[2] National Grid, NETS SQSS and Grid Code GSR018/GC0077: Sub-Synchronous Oscillations (SSO), U.K., Mar. 2017.

[3] P. M. Anderson, B. L. Agrawal, and J. E. Van Ness, Subsynchronous Resonance in Power Systems. Piscataway, NJ, USA: IEEE Press, 1990.

[4] K. R. Padiyar, Analysis of Subsynchronous Resonance in Power Systems. Boston, MA, USA: Kluwer, 1999.

[5] National Grid, System Operability Framework 2015, Nov. 2015.

[6] K. M. Alawasa and Y. A.-R. I. Mohamed, "A Simple Approach to Damp SSR in Series-Compensated Systems via Reshaping the Output Admittance of a Nearby VSC-Based System," IEEE Trans. Indust. Electron., vol. 62, no. 5, pp. 2673-2682, May 2015.

[7] D. Sun, X. Xie, Y. Liu, K. Wang and M. Ye, "Investigation of SSTI Between Practical MMC-Based VSC-HVDC and Adjacent Turbogenerators Through Modal Signal Injection Test," IEEE Trans. Power Del., vol. 32, no. 6, pp. 2432-2441, Dec. 2017.

[8] W. Du, Q. Fu, and H. Wang, "Subsynchronous Oscillations Caused by Open-Loop Modal Coupling Between VSC-Based HVDC Line and Power System," IEEE Trans. Power Syst., vol. 33, no. 4, pp. 3664-3677, July 2018.

[9] X. Xie, H. Liu, and Y. Han, "SEDC's Ability to Stabilize SSR: A Case Study on a Practical Series-Compensated Power System," IEEE Trans. Power Syst., vol. 29, no. 6, pp. 3092-3101, Nov. 2014.

[10] P. Dattaray, D. Chakravorty, P. Wall, J. Yu, and V. Terzija, "A Novel Control Strategy for Subsynchronous Resonance Mitigation Using 11 kV VFD-Based Auxiliary Power Plant Loads," *IEEE Trans. Power Del.* vol. 33, no. 2, pp. 728-740, Apr. 2018.

[11] X. Xie, L. Wang, and Y. Han, "Combined Application of SEDC and GTSDC for SSR Mitigation and Its Field Tests," *IEEE Trans. Power Syst.*, vol. 31, no. 1, pp. 769-776, Jan. 2016.

[12] T. Rauhala, A. M. Gole, and P. Järventausta, "Detection of Subsynchronous Torsional Oscillation Frequencies Using Phasor Measurement," *IEEE Trans. Power Del.*, vol. 31, no. 1, pp. 11-19, Feb. 2016.

[13] L. Livermore, C. E. Ugalde-Loo, Q. Mu, J. Liang, J. B. Ekanayake and N. Jenkins, "Damping of subsynchronous resonance using a voltage source converter-based high-voltage direct-current link in a series compensated Great Britain transmission network," *IET Gen. Trans. & Distr.*, vol. 8, no. 3, pp. 542-551, Mar. 2014.

[14] Q. Y. Jiang, Y. J. Cao, and S. J. Cheng, "A genetic approach to design a HVDC supplementary subsynchronous damping controller," *IEEE Trans. Power Del.*, vol. 20, no. 2, pp. 10591064, Apr. 2005.

[15] K. R. Padiyar and N. Prabhu, "Design and performance evaluation of subsynchronous damping controller with STATCOM," *IEEE Trans. Power Del.*, vol. 21, no. 3, pp. 1398-1405, Jul. 2006.

[16] R. J. Piwko and E. V. Larsen, "HVDC System Control for Damping of Subsynchronous Oscillations," *IEEE Trans. Power App. Syst.*, vol. 101, no. 7, pp. 2203-2211, Jul. 1982.

[17] C. McTaggart, D. Adam, C. Brozio, J. Stokoe, and R. Adobes, "The Application of Series Compensation to the Existing Scottish 400 kV Transmission System," *CIGRE C 4-125,* Paris Session, Sept. 2018.

[18] M. Bongiorno, J. Svensson, and L. Angquist, "Single-Phase VSC Based SSSC for Subsynchronous Resonance Damping," *IEEE Trans. Power Del.*, vol. 23, no. 3, pp. 1544-1552, Jul. 2008.

[19] T. Rajaram, J. M. Reddy and Y. Xu, "Kalman Filter Based Detection and Mitigation of Subsynchronous Resonance with SSSC," *IEEE Trans. Power Syst.*, vol. 32, no. 2, pp. 1400-1409, Mar. 2017.

[20] T. Joseph, C. E. Ugalde-Loo, S. Balasubramaniam, and J. Liang, "Real-Time Estimation and Damping of SSR in a VSC-HVDC Connected Series-Compensated System," *IEEE Trans. Power Syst.*, vol. 33, no. 6, pp. 7052-7063, Nov. 2018.

[21] X. Xie, L. Wang, X. Guo, Q. Jiang, Q. Liu, and Y. Zhao, "Development and Field Experiments of a Generator Terminal Subsynchronous Damper," *IEEE Trans. Power Electron.*, vol. 29, no. 4, pp. 1693-1701, April 2014.

[22] J. Zhang, X. Xiao, P. Zhang, C. Luo, Y. Wu, J. Lu and L. Ren, "Suppressing Intermittent Subsynchronous Oscillation via Subsynchronous Modulation of Reactive Current," *IEEE Trans. Power Del.*, vol. 30, no. 5, pp. 2321-2330, Oct. 2015.

[23] Interactions between HVDC systems and other connections, *ENTSO-E guidance document for national implementation for network codes on grid connection,* March 2018.

[24] C. E. Ugalde-Loo, J. B. Ekanayake and N. Jenkins, "Subsynchronous resonance in a series-compensated Great Britain transmission network," *IET Gen. Trans. & Distr.*, vol. 7, no. 3, pp. 209-217, Mar. 2013.

[25] T. Joseph, C. E. Ugalde-Loo, and J. Liang, "Subsynchronous Oscillatory Stability Analysis of an AC/DC Transmission System," in *Proc. IEEE Eindhoven PowerTech*, Eindhoven, Netherlands, 2015, pp. 1-6.

[26] F. M. Hughes, O. Anaya-Lara, N. Jenkins, and G. Strbac, "A power system stabilizer for DFIG-based wind generation," *IEEE Trans. Power Syst.*, vol. 21, no. 2, pp. 763-772, May 2006.

[27] C. E. Ugalde-Loo, J. B. Ekanayake, and N. Jenkins, "Subsynchronous resonance on series compensated transmission lines with quadrature boosters," in *Proc. IEEE Trondheim PowerTech*, Trondheim, Norway, 2011, pp. 802-808.

[28] GB Power System Modelling Capability Reports, IET Report for the Council of Science and Technology, Aug. 2017.

[29] A. Bostrom, "ABB FACTS Technology Developments," IEEE HVDC & FACTS Subcommittee, IEEE PES General Meeting, Portland, USA, Aug. 2018.

[30] C. Hor, J. Finn, G. Thumm, and S. Mortimer, "Introducing series compensation in the UK transmission network," in *Proc. 9th IET International Conference on AC and DC Power Transmission (ACDC 2010)*, London, UK, 2010, pp. 1-5.

[31] IEEE Subsynchronous Resonance Task Force of the Dynamic System Performance Working Group Power System Engineering Committee, "First benchmark model for computer simulation of subsynchronous resonance," *IEEE Trans. Power App. Syst.*, vol. 96, no. 5, pp. 1565-1572, Sept. 1977.

[32] IEEE Subsynchronous Resonance Working Group of the Dynamic System Performance Subcommittee Power System Engineering Committee, "Second Benchmark Model for Computer Simulation of Subsynchronous Resonance," *IEEE Trans. Power App. Syst.*, vol. 104, no. 5, pp. 1057-1066, May 1985.

[33] T. Joseph, C. E. Ugalde-Loo, J. Liang, and P. Coventry, "Active Filtering Based Current Injection Method for Multi Modal SSR Damping in an AC/DC System," in *Proc. 17th Euro. Conf. Power Electron. Appl. (EPE'15 ECCE-Europe)*, Geneva, Switzerland, 2015, pp. 1-10.

[34] "Flexible AC Transmission Systems: Series Compensation," Power Transmission and Distribution, Report, Siemens (2019). [online] Available at: http://www.siemens.co.in/pool/about_us/our_business_segments/facts_catalog.pdf, [Accessed 25 Jan. 2019].

[35] T. Rauhala, Subsynchronous oscillations – aspects and experiences from Finland. Energiforsk seminar: Subsynchronous oscillations, Stockholm, Nov. 2016.

[36] CIGRE WG Report, "Experience with Equipment for Series and Shunt Compensation," *CIGRE report, WG A3.33*, pp. 146, July 2017.

[37] P. Pourbeik, A. Bostrom, and B. Ray, "Modeling and application studies for a modern static VAr system installation," *IEEE Trans. Power Del.*, vol. 21, no. 1, pp. 368-377, Jan. 2006.

[38] EPRI, "Torsional Interaction Between Electrical Network Phenomena and Turbine-Generator Shafts: Plant Vulnerability," Palo Alto, USA, 2006.

[39] I. S. Sokhey, D. J. N. Limebeer, and D. C. Macdonald, "Turbine generator laboratory model tests to damp torsional oscillations with supplementary signals," *IEEE Trans. Energy Conver.*, vol. 8, no. 1, pp. 85-91, Mar. 1993.

[40] N. Prabhu and K. R. Padiyar, "Investigation of subsynchronous resonance with VSC based HVDC transmission systems," *IEEE Trans. Power Del.*, vol. 24, no. 1, pp. 433-440, Jan. 2009.

[41] K. R. Padiyar and N. Prabhu, "Investigation of SSR characteristics of unified power flow controller." *Electric Power Syst. Res.,* vol. 74, no. 2, pp. 211-221, May 2005.

[42] M. Bongiorno, J. Svensson and L. Angquist, "Online Estimation of Subsynchronous Voltage Components in Power Systems," *IEEE Trans. Power Del.*, vol. 23, no. 1, pp. 410-418, Jan. 2008.

[43] M. Janaki, N. Prabhu, R. Thirumalaivasan, "Mitigation of SSR by Subsynchronous Current Injection with VSC HVDC, *Intl. Journal of Electrical Power & Energy Syst.,* vol. 57, no. 1, pp. 287-297, May 2014.

[44] R. Nath and C. Grande-Moran, "Study of Sub-Synchronous Control Interaction due to the Interconnection of Wind Farms to a Series Compensated Transmission System," in *Proc. PES T&D 2012*, Orlando, USA, 2012, pp. 1-6.

Tibin Joseph (S'13-M'16) received the B.Tech. and M.Tech degrees in electrical engineering from Mahatma Gandhi University, Kerala, India, in 2008 and 2011, respectively. From 2012 to 2013 he worked as a Lecturer at Saintgits College of Engineering, Kerala, India. He obtained the Ph.D degree in electrical and electronic engineering from Cardiff University, Wales, U.K. in 2018.

He was a Marie Curie Early Stage Researcher between 2013 and 2016 at Cardiff University. He has been a visiting researcher at CEPRI in Beijing, China, and at National Grid, Warwick, U.K. Since 2016 he has been working as a Research Associate at Cardiff University.

Carlos E. Ugalde-Loo (M'02) was born in Mexico City. He received the B.Sc. degree in electronics and communications engineering from Instituto Tecnológico y de Estudios Superiores de Monterrey, Mexico City, México, in 2002, the M.Sc. degree in electrical engineering from Instituto Politécnico Nacional, Mexico City, México, in 2005, and the Ph.D. degree in electronics and electrical engineering from the University of Glasgow, Scotland, U.K., in 2009.

In 2010 he joined the School of Engineering in Cardiff University, Wales, U.K., and is currently Reader in Electrical Power Systems. His academic expertise includes power system stability and control, grid integration and control of renewables, HVDC transmission, integrated energy systems, modeling of dynamic systems, and multivariable control.

Senthooran Balasubramaniam (S'12-M'18) received the B.Eng. (Hons.) degree in electronic engineering from the University of Surrey, U.K., in 2012, and the Ph.D. degree in electrical and electronic engineering from Cardiff University, Wales, U.K., in 2017.

He is currently a Postdoctoral Researcher with the Energy Safety Research Institute in Swansea University, Wales, U.K. His main research interests include HVDC technologies, power electronics, grid integration of renewable energy, and power system control and stability.

Jun Liang (M'02-SM'12) received the B.Sc. degree from Huazhong University of Science and Technology, Wuhan, China, in 1992 and the M.Sc. and Ph.D. degrees from China Electric Power Research Institute, Beijing, China, in 1995 and 1998, respectively. From 1998 to 2001 he was a Senior Engineer with China Electric Power Research Institute. From 2001 to 2005 he was a Research Associate at Imperial College, London, U.K. From 2005 to 2007 he was a Senior Lecturer at the University of Glamorgan, Wales, U.K.

He is currently a Professor at the School of Engineering, Cardiff University, Wales, U.K. He is an Editorial Board Member of CSEE JPES. His research interests include FACTS devices/HVDC, power system stability and control, power electronics, and renewable power generation.

Gen Li received the B.Eng. degree from Northeast Electric Power University, Jilin, China, in 2011, the M.Sc. degree from Nanyang Technological University, Singapore, in 2013 and the Ph.D. degree from Cardiff University, Cardiff, U.K., in 2018.

From 2013 to 2016, he was a Marie Curie Early Stage Researcher funded by European Union's MEDOW project. He has been a Visiting Researcher at China Electric Power Research Institute, Beijing, China, at Elia, Brussels, Belgium and at Toshiba International (Europe), London, U.K. He has been a Research Associate at the School of Engineering, Cardiff University, Cardiff, U.K., since 2017. His research interests include high voltage and medium voltage dc technologies, power electronics and power system stability control.